Inorganic Chemistry

ARTICLE

pubs.acs.org/IC

Temperature and Pressure Evolution of the Crystal Structure of $A_x(Fe_{1-y}Se)_2$ (A = Cs, Rb, K) Studied by Synchrotron Powder Diffraction

V. Svitlyk,*[,†] D. Chernyshov,[†] E. Pomjakushina,[‡] A. Krzton-Maziopa,[‡] K. Conder,[‡] V. Pomjakushin,[§] and V. Dmitriev[†]

[†]Swiss-Norwegian Beamlines at European Synchrotron Radiation Facility, BP 220, 38043 Grenoble, France

[‡]Laboratory for Developments and Methods, PSI, CH-5232 Villigen PSI, Switzerland

[§]Laboratory for Neutron Scattering, Paul Scherrer Institute, CH-5232 Villigen PSI, Switzerland

ABSTRACT:

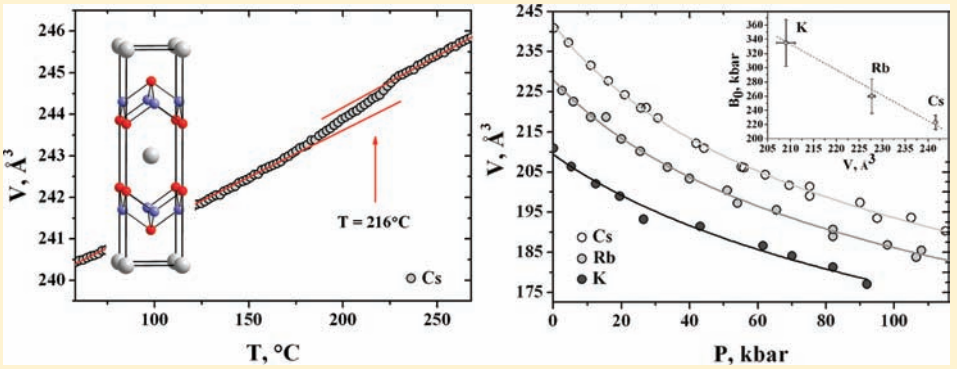

Temperature-dependent synchrotron powder diffraction on $Cs_{0.83}(Fe_{0.86}Se)_2$ revealed first-order $I4/m$ to $I4/mmm$ structural transformation around 216 °C associated with a disorder of the Fe vacancies. Irreversibility observed during the transition is likely associated with a mobility of the intercalated alkali atoms. Pressure-dependent synchrotron powder diffraction on $Cs_{0.83}(Fe_{1-y}Se)_2$, $Rb_{0.85}(Fe_{1-y}Se)_2$, and $K_{0.8}(Fe_{1-y}Se)_2$ ($y \sim 0.14$) indicated that the $I4/m$ superstructure reflections are present up to pressures of 120 kbar. This may indicate that the ordering of the Fe vacancies is present in both superconducting and nonsuperconductive states.

1. INTRODUCTION

The discovery of superconductivity in $Cs_x(Fe_{1-y}Se)_2$, $Rb_x(Fe_{1-y}Se)_2$, and $K_x(Fe_{1-y}Se)_2$[1−3] is one more step on the way to comprehending the mechanism of superconductivity in a family of layered Fe-based compounds. Very recently, it was found that these compounds are magnetically ordered at room temperature and remain ordered in a superconducting state;[4] this is a rather unusual property for a superconductor. Another, also to a certain extent unique, structural feature is an ordering of the Fe vacancies in the FeSe superconducting layer, initially suggested in 1986[5,6] and recently confirmed by single crystal synchrotron, neutron powder, and laboratory X-ray single crystal diffraction studies.[7,8] The ordering is manifested as a set of weak superstructure reflections with propagation vector star [2/5,1/5,1] that disappear on heating, thus indicating an onset of the order−disorder transition.[7] An ordered pattern of the Fe vacancies together with magnetism are considered important components of superconductivity.[9,10]

Different possible structural models of ordering of Fe vacancies were reported before. The structural model in the $I4/m$ symmetry with a $\sqrt{5} \times \sqrt{5} \times 1$ super cell and 5 times larger volume compared to the basic $I4/mmm$ unit cell, the $ThCr_2Si_2$-type structure, dominates in the literature.[7,8,11−13] Other reported models correspond to a super cell with **q**-vector **q1** = [3/5, 1/5, 0] and coexisting vectors **q1** and **q2** = [3/4, 1/4, 0].[14] The $5 \times 5 \times 1$ super cell was also reported[15] with a further revision in a $\sqrt{5} \times \sqrt{5} \times 1$ super cell.[8] The orthorhombic $Pmna$ structure with $\sqrt{2} \times \sqrt{2} \times 1$ unit cell dimensions of the $ThCr_2Si_2$-type basic cell was observed together with the $I4/mmm$ and $I4/m$ structures.[16] However, a symmetry-based phenomenological analysis enumerating possible ordering patterns within a unified scheme is not reported; there is also no agreement on the order of the transition, since structural features characteristic for both, first and second order transitions, are seen in the diffraction experiments.[7,13]

A number of pressure-dependent studies on the structures and ordering temperatures of the layered Fe-based systems were carried out.[17−27] Very recently, the first pressure-dependent studies on the conductivity of $Cs_x(Fe_{1-y}Se)_2$ revealed a suppression of the superconductivity at pressures of about 80 kbar.[28] However, studies of structural behavior as a function of pressure have not yet been done for the $Cs_x(Fe_{1-y}Se)_2$, $Rb_x(Fe_{1-y}Se)_2$, and $K_x(Fe_{1-y}Se)_2$ phases.

Received: May 30, 2011
Published: October 11, 2011

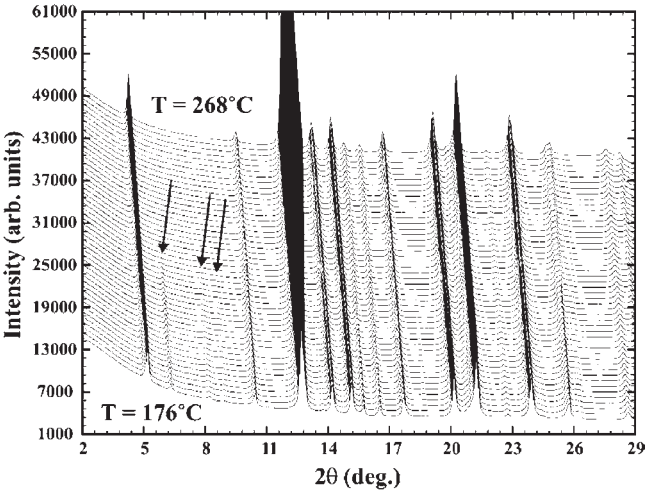

Figure 1. Powder diffraction data as a function of temperature collected for the $Cs_{0.83}(Fe_{0.86}Se)_2$ sample (data in the 176−268 °C temperature range are shown). The arrows mark the vanishing of the superstructure (110), (112), and (020) reflections upon heating, which are indicative of the Fe vacancies ordering.

Numerous electronic structure calculations for these and related compounds appeared as well,[29−35] not necessarily in agreement with the experimental data. In fact, it is not completely proper to put side by side a theoretical model obtained for a temperature of 0 K and a real room-temperature structure as found in diffraction experiments, especially with the presence of structural disorder. The robust link and, at the same time, the control parameters between theory and practice can be a bulk modulus and thermal expansion coefficient, which can be obtained independently theoretically and experimentally. Corresponding experimental data have also not been reported so far.

Therefore, in spite of the great interest in the new family of superconductors, there are still many open questions related to the phase transition phenomena and basic physical properties. In order to close these gaps, we have systematically studied pressure and temperature evolution of the crystal structure of $Cs_x(Fe_{1-y}Se)_2$, $Rb_x(Fe_{1-y}Se)_2$, and $K_x(Fe_{1-y}Se)_2$ with the help of synchrotron radiation.

In this paper, we present the first experimental results of the pressure-dependent X-ray powder diffraction on $Cs_{0.83}(Fe_{1-y}Se)_2$, $Rb_{0.85}(Fe_{1-y}Se)_2$, and $K_{0.8}(Fe_{1-y}Se)_2$ ($y \sim 0.14$). The data collected as a function of pressure have been parametrized in the form of the equation of state, thus giving the first experimental estimates of the bulk moduli. We also show that pressure does not suppress the ordering of iron vacancies even at high pressures where no superconductivity is expected to survive. We report a detailed temperature dependence of the order parameter for $Cs_{0.83}(Fe_{0.86}Se)_2$ responsible for the ordering of the vacancies in the iron sublattice; we show also that the sample's decomposition could go in parallel with the phase transformation. Our experimental findings are complemented with a symmetry-based phenomenological consideration of the observed phase transformation to link together numerous and sometime contradictory results reported so far.

2. EXPERIMENTAL PROCEDURE

Single crystals of the $Cs_x(Fe_{1-y}Se)_2$, $Rb_x(Fe_{1-y}Se)_2$, and $K_x(Fe_{1-y}Se)_2$ samples studied in this work are the same as those in ref 7. The crystals were grown using the Bridgman method, and the details of the experimental procedure are given in ref 2.

2.1. X-Ray Fluorescence Spectroscopy. Homogeneity and elemental composition of the cleaved crystals were studied using X-ray fluorescence spectroscopy (XRF, Orbis Micro-XRF Analyzer, EDAX). Elemental distribution maps for K, Rb, Cs, Fe, and Se were collected in a vacuum applying white X-ray radiation produced by a Rh tube (35 kV and 500 μA). The X-ray primary beam was focused to a spot of 30 μm diameter. A primary beam Ti filter (25 μm thickness) was applied. An area of ~0.5 cm^2 was scanned. Prior to the measurements, elemental calibration was done using as a standard carefully weighted, homogenized, and pressed into a pellet mixture of Se, Fe, and corresponding alkali metal carbonates. The applied calibration procedure results in ~2% accuracy of the determined stoichiometric coefficient values.

2.2. Temperature- and Pressure-Dependent Powder Diffraction. For temperature-dependent powder diffraction, single crystals of the $Cs_{0.83}(Fe_{1-y}Se)_2$ sample were finely ground and sealed in quartz capillaries in a glovebox under an argon atmosphere. During the diffraction experiment, the temperature was changed in the 58−268 °C temperature range with a 2 °C step on heating (Figure 1) and on cooling to check for possible structural hysteresis.

For pressure-dependent powder diffraction, single crystals of the $Cs_{0.83}(Fe_{1-y}Se)_2$, $Rb_{0.85}(Fe_{1-y}Se)_2$, and $K_{0.8}(Fe_{1-y}Se)_2$ samples were finely ground in the glovebox under an argon atmosphere as well. Sealed samples were opened immediately before loading to the high pressure (HP) diamond anvil cells to minimize exposure to the air. Silicon oil AP 100 was used as a pressure transmitting medium. A typical ethanol−methanol mixture, which retains good hydrostaticity at pressures up to 100 kbar, could not be used due to a high chemical reactivity with the samples. During diffraction experiments, pressure was changed from 0 to 100−120 kbar, depending on a sample tolerance, with a typical step of 5 kbar on loading and 20 kbar on unloading. The samples were contained by stainless steel gaskets with holes of 0.3 mm in diameter, the pressure was calculated from the shift in the fluorescence signals from the added ruby crystals.

Both temperature- and pressure-dependent data collections were performed on the MAR345 diffractometer using synchrotron radiation with $\lambda = 0.69775$ Å. Data were integrated and processed with the FIT2D software;[36,37] standard deviations were calculated with local software. Powder data were refined with the FullProf software.[38]

3. RESULTS AND DISCUSSION

3.1. Compositions of the $A_x(Fe_{1-y}Se)_2$ (A = Cs, Rb, K) Samples. Composition for the Cs-based compound obtained during the previous single crystal diffraction experiment is equal to $Cs_{0.83(1)}(Fe_{0.86(1)}Se)_2$.[7] Compositions for the Cs-, Rb-, and K-containing samples obtained from the room temperature synchrotron powder diffraction data are $Cs_{0.70(1)}(Fe_{0.82(1)}Se)_2$, $Rb_{0.66(1)}(Fe_{0.84(1)}Se)_2$, and $K_{0.59(1)}(Fe_{0.87(1)}Se)_2$. Finally, the chemical compositions obtained from the XRF analysis are $Cs_{0.74}(Fe_{0.77}Se)_2$, $Rb_{0.77}(Fe_{0.81}Se)_2$, and $K_{0.68}(Fe_{0.85}Se)_2$, with an overall accuracy of about 2%. Nonconsistency of the chemical compositions obtained from the different methods likely originates both from the different character of the samples, i.e., single crystals or powder, and from experimental peculiarities of the specific technique. While both single crystal and powder diffraction methods are bulk probes, powdered samples could overall differ in compositions from single crystalline samples due to a large effective surface area. This could be a particularly crucial factor for the $A_x(Fe_{1-y}Se)_2$ phases with the intercalated and mobile alkali atoms. To the contrary, the XRF technique is a

dx.doi.org/10.1021/ic201160y |Inorg. Chem. 2011, 50, 10703–10708

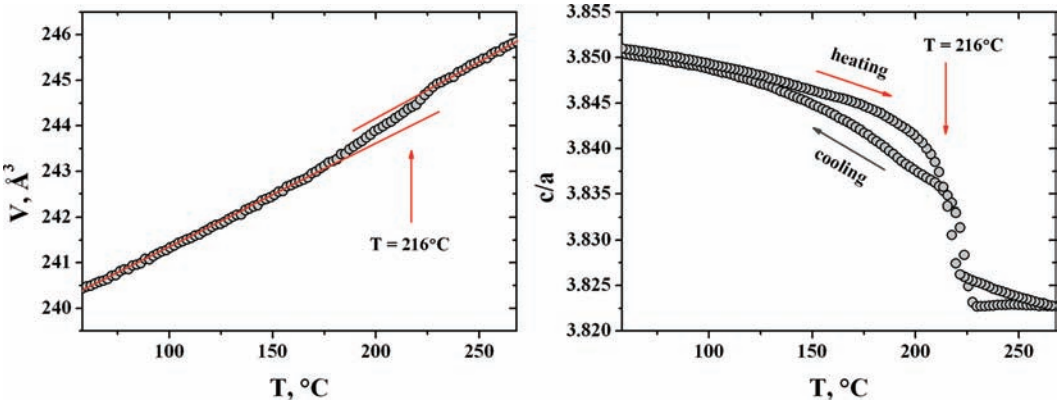

Figure 2. Dependence of the unit cell volume of $Cs_{0.83}(Fe_{1-y}Se)_2$ (left) and the c/a parameters ratio (right) vs temperature.

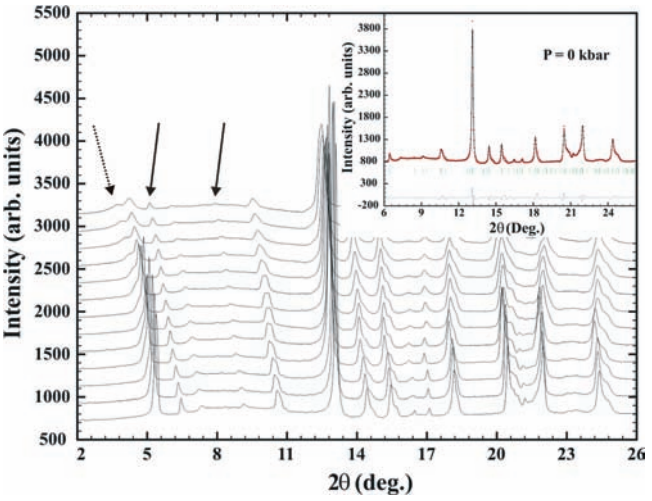

Figure 3. Powder diffraction data as a function of pressure, from ambient pressure (bottom) to 123 kbar (top) for the $Rb_{0.85}(Fe_{1-y}Se)_2$ sample. The solid arrows indicate (110) and (020) superstructure reflections. The dotted arrow indicates the impurity peak. The inset shows an example of the structure refinement of the ambient pressure data set within the $I4/m$ model.

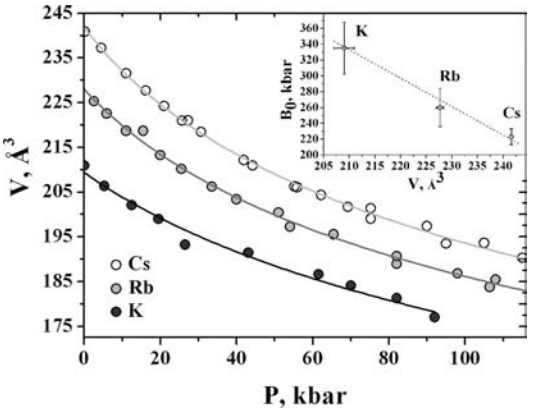

Figure 4. Volume vs pressure dependences for $Cs_{0.83}(Fe_{1-y}Se)_2$, $Rb_{0.85}(Fe_{1-y}Se)_2$, and $K_{0.8}(Fe_{1-y}Se)_2$ fitted with the Murnaghan equation of state. The inset shows bulk moduli versus the unit cell volumes at ambient pressure.

surface probe. For simplicity, we use a notation for the Cs-containing sample of $Cs_{0.83}(Fe_{1-y}Se)_2$ and a nominal one for alkali metals for Rb- and K-containing samples, i.e., $Rb_{0.85}(Fe_{1-y}Se)_2$ and $K_{0.8}(Fe_{1-y}Se)_2$, throughout the text.

3.1. Thermal Expansion of $Cs_{0.83}(Fe_{1-y}Se)_2$. Order−disorder transition in the $Cs_{0.83}(Fe_{1-y}Se)_2$ phase can be observed in the temperature-dependent powder patterns as a vanishing of superstructure reflections (Figure 1).

The temperature dependence of the unit cell volume of $Cs_{0.83}(Fe_{1-y}Se)_2$ is presented in Figure 2, left (the data collected on heating are shown; the error bars are not shown when their size is the same or smaller than the size of the corresponding graphical markers).

An anomaly around T = 216 °C corresponds to a transition from the $I4/m$ structure with the ordered Fe vacancies to the basic $ThCr_2Si_2$-type $I4/mmm$ structure with disordered Fe vacancies.[7] The linear coefficients of thermal expansion, $\alpha = 1/V_0((V - V_0)/(T - T_0))$, with V_0 (V) and T_0 (T), the initial (final) unit cell volume and the sample temperature, being 9.26×10^{-5} (T interval 58−167 °C) and 9.93×10^{-5} °C^{-1} (T interval 234−268 °C) for the low-temperature $I4/m$ and high-temperature $I4/mmm$ structures, respectively. Some information on the temperature evolution of the unit cell dimensions was reported by us earlier;[7] here, we complement it with the unit cell ratio, indicating rather anisotropic thermal expansion. One could see that all observed dependences agree with a first order character of the phase transition. Interestingly, there are broad hysteresis zones both above and below the transition temperature.

3.2. Equations of State and Bulk Modules for $Cs_{0.83}(Fe_{1-y}Se)_2$, $Rb_{0.85}(Fe_{1-y}Se)_2$, and $K_{0.8}(Fe_{1-y}Se)_2$. The best tolerance to the HP was exhibited by the $Rb_{0.85}(Fe_{1-y}Se)_2$ sample, followed by the $Cs_{0.83}(Fe_{1-y}Se)_2$ and $K_{0.8}(Fe_{1-y}Se)_2$ samples. The poor hydrostaticity of silicon oil resulted in high induced strains in the samples at high pressures. As a result, powder data for all samples were treated in the average $I4/mmm$ structures. The Cs and Fe occupancies in the $Cs_{0.83}(Fe_{1-y}Se)_2$, $Rb_{0.85}(Fe_{1-y}Se)_2$, and $K_{0.8}(Fe_{1-y}Se)_2$ phases could not be reliably refined from the experimental powder data.

For all samples, a peak of an unidentified secondary phase was seen at low angles close to the position of the 002 reflection (indexed in $I4/m$) (Figure 3). The peak was disregarded and omitted from the refinement; most probably it comes from a secondary phase as a result of samples' surface

dx.doi.org/10.1021/ic201160y |Inorg. Chem. 2011, 50, 10703–10708

degradation. A similar observation has been reported before[39] and ascribed to an inhomogeneous distribution of intercalated ions.

Volume versus pressure dependences for the $Cs_{0.83}(Fe_{1-y}Se)_2$, $Rb_{0.85}(Fe_{1-y}Se)_2$, and $K_{0.8}(Fe_{1-y}Se)_2$ samples (*I*4/*mmm* setting) fitted with the Murnaghan equation of state (eq 1, V_0 is the volume at zero pressure, B_0 is the bulk modulus, and B_0' is the first pressure derivative of the bulk modulus) are shown in Figure 4. Fitted parameters are summarized in Table 1.

$$V(P) = V_0\left(1 + B_0'\frac{P}{B_0}\right)^{1/B_0'} \quad (1)$$

Since the ionic radius of alkali ions increases from K to Cs, an increase of the V_0 is expected and agrees with the observation. A decrease in the bulk modulus with the increase in the ionic radius is less obvious and may even be considered counterintuitive. It is, however, also expected if we account for the stoichiometry—by adding bigger alkali ions, we also create larger vacancy voids in this sublattice, thus making the structure less dense and therefore more compressive. As a result, we observe an inverse correlation between the bulk moduli and the unit cell volumes at ambient pressure (Figure 4, inset).

3.3. Temperature and Pressure-Dependent Crystallographic Behavior of $Cs_{0.83}(Fe_{1-y}Se)_2$, $Rb_{0.85}(Fe_{1-y}Se)_2$, and $K_{0.8}(Fe_{1-y}Se)_2$. First, we should note a lack of a complete reversibility in the temperature and pressure scans. Temperature-dependent anomalies in $Cs_{0.83}(Fe_{1-y}Se)_2$ related to the order−disorder phase transition could be observed starting at 216 °C on heating (Figure 5). The most prominent changes were exhibited by the *c* cell parameter, Se *z* coordinate, and correspondingly the height of Se atoms (Figure 5, right). For the Fe-based superconductors, the latter parameter is considered an important one for structure−property correlations[40] and is defined as a distance between the Se and Fe layers; the $A_x(Fe_{1-y}Se)_2$ phases belonging to the $ThCr_2Si_2$-type structure can be viewed as constructed from layers of atoms of the same kind.

While hysteresis indicates a first order of the transition near 216 °C, irreversibility of the temperature evolution might be related to a certain mobility of Cs cations, even within a sealed capillary. One, therefore, has to avoid diffraction experiments under a dynamic vacuum to prevent possible changes in the stoichiometry.

Dependence of the anion height on the pressure can be used as a convenient tool to track possible changes in the conductivity of samples.[40] In our case, no pronounced pressure-dependent anomalies have been found for the $Cs_{0.83}(Fe_{1-y}Se)_2$, $Rb_{0.85}(Fe_{1-y}Se)_2$, and $K_{0.8}(Fe_{1-y}Se)_2$ samples. A big spread of experimental data points was observed that probably originates from the correlations between structural parameters unavoidably appearing due to the quality of diffraction patterns limited by the high-pressure experiment.

The *I*4/*m* superstructure peaks did not disappear on applying the pressure in the $Cs_{0.83}(Fe_{1-y}Se)_2$, $Rb_{0.85}(Fe_{1-y}Se)_2$, and $K_{0.8}(Fe_{1-y}Se)_2$ samples. This indicates that the ordering of the Fe vacancies was not suppressed within the range of applied pressures.

3.4. Phenomenological Analysis of Order−Disorder Phase Transition. Analysis of the possible structural transformations in $A_x(Fe_{1-y}Se)_2$ following a symmetry-based phenomenological scheme is needed to validate the experimentally obtained models. Accurate single-crystal diffraction experiments[7] show that the structural distortion, which is the ordering of the iron vacancies, propagates with a reciprocal space vector $\mathbf{k}_{2i}$ = [2/5, 1/5, 1] which is identical to $\mathbf{k}_{2p}$ = [2/5, −2/5, 4/5] and corresponds to the Θ point of the tetragonal Brillouin zone (BZ). We use hereafter reciprocal **k** vectors both in the notations of the International Tables for Crystallography[41] (denoted by index "i") dominating in the experimental works and in the primitive basis according to ref 42, which is mainly conventional in the group-theoretical exercises. Basis transformation from the parent Bravais lattice (lowercase letters) to the distorted one reads

$$\mathbf{A} = 2\mathbf{a} + \mathbf{b}; \mathbf{B} = -\mathbf{a} + 2\mathbf{b}; \mathbf{C} = \mathbf{c} \quad (2)$$

Vectors in eq 2 identify two body-centered tetragonal Bravais cells. Orientational relationships between the corresponding

Table 1. Experimental Coefficients of the Murnaghan Equation of State for $Cs_{0.83}(Fe_{1-y}Se)_2$, $Rb_{0.85}(Fe_{1-y}Se)_2$, and $K_{0.8}(Fe_{1-y}Se)_2$ Obtained from the Pressure-Dependent Synchrotron X-Ray Powder Diffraction (*I*4/*mmm* settings)

sample	V_0, Å^3	B_0, kbar	B_0'
$Cs_{0.83}(Fe_{1-y}Se)_2$	241.6(3)	223(10)	5.8(3)
$Rb_{0.85}(Fe_{1-y}Se)_2$	227.7(7)	260(24)	5.9(7)
$K_{0.8}(Fe_{1-y}Se)_2$	209(2)	335(33)	5.8 (fixed)

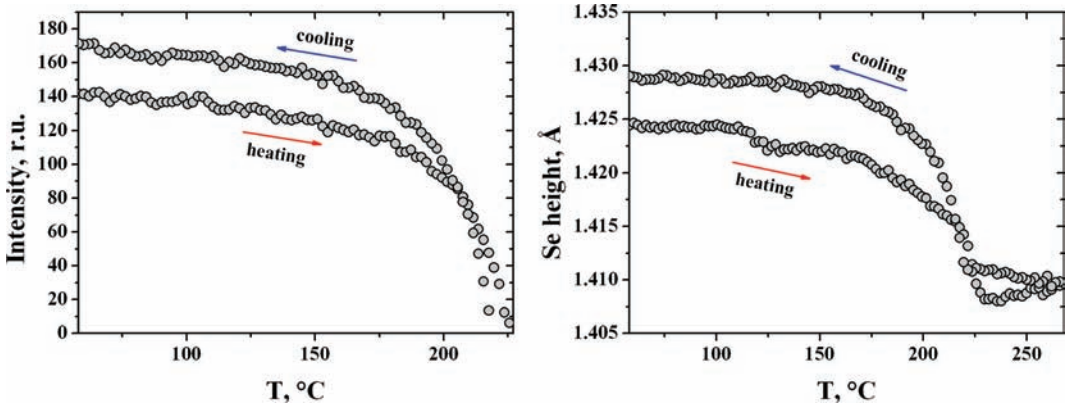

Figure 5. Temperature dependence of intensity of the 110 superstructure reflection (*I*4/*m*; left) and the height of Se atoms in the FeSe layer (right, errors average is equal to 4×10^{-3}) in $Cs_{0.83}(Fe_{1-y}Se)_2$.

dx.doi.org/10.1021/ic201160y |*Inorg. Chem.* 2011, 50, 10703–10708

primitive (independent) unit cells look as follows:

$$\mathbf{d}_1 = \mathbf{a}_1 - \mathbf{a}_2 - \mathbf{a}_3, \mathbf{d}_2 = 2\mathbf{a}_2 + \mathbf{a}_3, \mathbf{d}_3 = \mathbf{a}_1 + 2\mathbf{a}_3 \quad (3)$$

The basal vectors (**A**, **B**, **C**) of the distorted tetragonal structure (eq 2) are not parallel either to the same vectors (**a**, **b**, **c**) in the parent lattice or to its diagonal directions. It should result in the loss of the corresponding mirror planes parallel to and rotation axes perpendicular to the 4-fold axis in the distorted structure. A maximal crystal class for the low-symmetry structure can be therefore identified as $4/m$. Taking into account the systematic absences conditions, indicating a body-centered lattice for the low-symmetry phase, the space group $I4/m$ is suggested. Among other candidates, $P4_2/n$ with the same Bravais cell parameters (eq 2) could be considered. However, the corresponding phase transformation $I4/mmm-P4_2/n$ (unit cell volume multiplication $V'/V = 10$) involves, in addition to the above-mentioned distortion propagating with the $\mathbf{k}_2$, one more order parameter characterized by $\mathbf{k}_{15i} = [0, 0, 1/2]$. Careful investigations conclude the absence of the corresponding reflections violating *I*-centering in the diffraction patterns of the studied compounds.

Another candidate, which already appeared in earlier publications but later was rejected,[8,15] is the $I4/mmm$ structure with the unit cell volume multiplied by a factor of 25 with respect to the parent structure. Basis transformations between the crystal lattices are

$$\mathbf{A}' = 5\mathbf{a}; \mathbf{B}' = 5\mathbf{a}; \mathbf{C}' = \mathbf{c} \quad (4)$$

indicating that all eight arms of the vector star $\mathbf{k}_2$ participate in the propagation of the distortions during the $I4/mmm-I4/mmm$ ($V'/V = 25$) phase transition. It should manifest, in turn, in identical intensity of all eight satellites of the $\pm[2/5\ 1/5\ 1]$ type. In contrast, the superstructure in the $I4/m$ phase is formed by four out of eight star vectors: $\mathbf{k}_{2p}^{(1,2)} = \pm[2/5, -2/5, 4/5]$ and $\mathbf{k}_{2p}^{(3,4)} = \pm[4/5, 1/5, -2/5]$, and the condition of the equal intensities is satisfied in two quartets of the reflections, each corresponding to the different system of translational (antiphase, in other terminology) domains.[7,8]

For the sake of completeness, it is worth mentioning an orthorhombic structure found by the authors of ref 16. An additional phase described by the space group *Pmna* with a supercell of $\sqrt{2} \times \sqrt{2} \times 1$ of the tetragonal parent $I4/mmm$ was reported to exist in some samples between 295 and 500 K. Our analysis concludes that the corresponding structure distortion should propagate with $\mathbf{k}_{13i} = [1/2, 1/2, 0]$. A corresponding structural order parameter belongs to the X point [1/2 1/2 0] of the tetragonal BZ. Moreover, temperature treatment of the corresponding samples proves a metastable character of the *Pmna* structure, which is sensitive to the sample preparation conditions. The orthorhombic phase never appeared in our syntheses, and only single-phase samples were used in the present experiments.

4. CONCLUSIONS

Temperature ($Cs_{0.83}(Fe_{1-y}Se)_2$) and pressure evolution of the crystal structures ($Cs_{0.83}(Fe_{1-y}Se)_2$, $Rb_{0.85}(Fe_{1-y}Se)_2$, and $K_{0.8}(Fe_{1-y}Se)_2$) were studied using synchrotron powder diffraction. The structure of $Cs_{0.83}(Fe_{1-y}Se)_2$ possesses the phase transition on heating related to the disorder of the iron vacancies in the FeSe layer, as we have shown before and in agreement with other reports.[7,16] At variance with the results reported in ref 14, we found the transition to be of the first order, as evidenced by hysteresis in the lattice properties and also agreeing with the differential scanning calorimetry.[7] At the same time, we have noted an irreversibility of the temperature dependences of the lattice constants and Bragg intensities. We tentatively relate the irreversibility to a mobility of the intercalating alkali ions; such mobility may seriously affect apparent temperature evolution of the crystal structure.

Our symmetry-based phenomenological analysis enumerates crystal structures reported so far. Among them, $I4/mmm$ can be considered the parent one, and two possible structures are associated with the vector star $\mathbf{k}_2$, $I4/m$ and $I4/mmm$. The formation of the hypothetical $P4_2/n$ structure involves, in addition to the above-mentioned distortion propagating with $\mathbf{k}_2$, one more order parameter characterized by the $\mathbf{k}_{15}$ wave vector. The orthorhombic *Pmna* structure with a $\sqrt{2} \times \sqrt{2} \times 1$ unit cell dimensions can be obtained from the parent one by the distortion associated with the $\mathbf{k}_{13}$ wave vector; a coexistence of this phase with the parent $I4/mmm$ and $I4/m$ ($\mathbf{k}_2$) reported in ref 16 is rather unusual and has to be confirmed by single crystal diffraction experiments. Symmetry imposes no constraints on the order of the transition between parent $I4/mmm$ and $I4/m$ ($\mathbf{k}_2$), $I4/mmm$ ($\mathbf{k}_2$), and $P4_2/n$ ($\mathbf{k}_2$, $\mathbf{k}_{15}$) structures; our experimental data indicate rather pronounced first order transition between $I4/mmm$ and $I4/m$ ($\mathbf{k}_2$) structures. One has, however, to take the temperature evolution of the structure and especially of the order parameter with a grain of salt, since the critical dependence may be strongly affected by the temperature variation of the sample's composition. Our experiment shows that such variation takes place even in a sealed capillary; the effect is expected to be much more pronounced if a sample has been heated under vacuum conditions during data collection.

In spite of numerous experimental problems related to the sample composition, homogeneity, and reactivity, our diffraction experiments as a function of pressure allowed us to recover the equation of states and, for the first time, provide the experimental estimates of the bulk moduli for the title compounds. Together with the thermal expansion coefficients calculated from the temperature-dependent diffraction, these data may serve as constraints for theoretical models. We have also seen that the Bragg reflections indicative of the ordering of the Fe vacancies in the FeSe layer do not disappear up to ~120 kbar. No clear anomaly for $Cs_{0.83}(Fe_{1-y}Se)_2$, $Rb_{0.85}(Fe_{1-y}Se)_2$, and $K_{0.8}(Fe_{1-y}Se)_2$ were observed around 80 kbar, where transport experiments indicate an offset of superconductivity; this conclusion, however, may be limited by the quality of the data. Albeit a definitive answer can only be obtained from diffraction experiments at high pressure and very low temperatures, our data assume that the ordering of the vacancies in the FeSe layer may be present in both superconducting and nonsuperconducting states.

AUTHOR INFORMATION

Corresponding Author

*E-mail: svitlyk@esrf.fr.

ACKNOWLEDGMENT

A.K.-M. acknowledges the support from the Scientific Exchange Programme Sciex-NMSch (Project Code 10.048) and E. P. acknowledges the support from the NCCR MaNEP Project.

REFERENCES

(1) Guo, J.; Jin, S.; Wang, G.; Wang, S.; Zhu, K.; Zhou, T.; He, M.; Chen, X. *Phys. Rev. B* **2010**, *82*, 180520.

(2) Krzton-Maziopa, A.; Shermadini, Z.; Pomjakushina, E.; Pomjakushin, V.; Bendele, M.; Amato, A.; Khasanov, R.; Luetkens, H.; Conder, K. *J. Phys.-Condens. Mater.* **2011**, *23*, 052203.

(3) Wang, A.; Ying, J.; Yan, Y.; Liu, R.; Luo, X.; Li, Z.; Wang, X.; Zhang, M.; Ye, G.; Cheng, P.; Xiang, Z.; Chen, X. *Phys. Rev. B* **2011**, *83*, 060512.

(4) Shermadini, Z.; Krzton-Maziopa, A.; Bendele, M.; Khasanov, R.; Luetkens, H.; Conder, K.; Pomjakushina, E.; Weyeneth, S.; Pomjakushin, V.; Bossen, O.; Amato, A. *Phys. Rev. Lett.* **2011**, *106*, 117602.

(5) Häggström, L.; Verma, H. R.; Bjarman, S.; Wäppling, R.; Berger, R. *J. Solid State Chem.* **1986**, *63*, 401.

(6) Sabrowsky, H.; Rosenberg, M.; Welz, D.; Deppe, P.; Schäfer, W. *J. Magn. Magn. Mater.* **1986**, *54*−*57*, 1497.

(7) Pomjakushin, V. Y.; Sheptyakov, D. V.; Pomjakushina, E. V.; Krzton-Maziopa, A.; Conder, K.; Chernyshov, D.; Svitlyk, V.; Shermadini, Z. *Phys. Rev. B* **2011**, *83*, 144410.

(8) Zavalij, P.; Bao, W.; Wang, X. F.; Ying, J. J.; Chen, X. H.; Wang, D. M.; He, J. B.; Wang, X. Q.; Chen, G. F.; Hsieh, P.-Y.; Huang, Q.; Green, M. A. *Phys. Rev. B* **2011**, *83*, 132509.

(9) Yan, Y. J.; Zhang, M.; Wang, A. F.; Ying, J. J.; Li, Z. Y.; Qin, W.; Luo, X. G.; Li, J. Q.; Hu, J.; Chen, X. H. arXiv: 1104.4941v1, 2011.

(10) Mazin, I. *Physics* **2011**, *4*, 26.

(11) Häggström, L.; Seidel, A.; Berger, R. *J. Magn. Magn. Mater.* **1991**, *98*, 37.

(12) Bacsa, J.; Ganin, A. Y.; Takabayashi, Y.; Christensen, K. E.; Prassides, K.; Rosseinsky, M. J.; Claridge, J. B. *Chem. Sci.* **2011**, *2*, 1054.

(13) Bao, W.; Huang, Q.; Chen, G. F.; Green, M. A.; Wang, D. M.; He, J. B.; Wang, X. Q.; Qiu, Y. arXiv:1102.0830v1, 2011.

(14) Wang, Z.; Song, Y. J.; Shi, H. L.; Wang, Z. W.; Chen, Z.; Tian, H. F.; Chen, G. F.; Guo, J. G.; Yang, H. X.; Li, J. Q. *Phys. Rev. B* **2011**, *83*, 140505(R).

(15) Zavalij, P.; Bao, W.; Wang, X. F.; Ying, J. J.; Chen, X. H.; Wang, D. M.; He, J. B.; Wang, X. Q.; Chen, G. F.; Hsieh, P.-Y.; Huang, Q.; Green, M. A. arXiv:1101.4882v1, 2011.

(16) Bao, W.; Li, G. N.; Huang, Q.; Chen, G. F.; He, J. B.; Green, M. A.; Qiu, Y.; Wang, D. M.; Luo, J. L. arXiv:1102.3674v1, 2011.

(17) Mizuguchi, Y.; Tomioka, F.; Tsuda, S.; Yamaguchi, T.; Takano, Y. *Appl. Phys. Lett.* **2008**, *93*, 152505.

(18) Margadonna, S.; Takabayashi, Y.; Ohishi, Y.; Mizuguchi, Y.; Takano, Y.; Kagayama, T.; Nakagawa, T.; Takata, M.; Prassides, K. *Phys. Rev. B* **2009**, *80*, 064506.

(19) Medvedev, S.; McQueen, T. M.; Troyan, I. A.; Palasyuk, T.; Eremets, M. I.; Cava, R. J.; Naghavi, S.; Casper, F.; Ksenofontov, V.; Wortmann, G.; Felser, C. *Nat. Mater.* **2009**, *8*, 630.

(20) Horigane, K.; Takeshita, N.; Lee, C. H.; Hiraka, H.; Yamada, K. *J. Phys. Soc. Jpn.* **2009**, *78*, 063705.

(21) Huang, C. L.; Chou, C. C.; Tseng, K. F.; Huang, Y. L.; Hsu, F. C.; Yeh, K. W.; Wu, M. K.; Yang, H. D. *J. Phys. Soc. Jpn.* **2009**, *78*, 084710.

(22) Sidorov, V. A.; Tsvyashchenko, A. V.; Sadykov, R. A. *J. Phys., Condens. Mater.* **2009**, *21*, 415701.

(23) Jorgensen, J. E.; Hansen, T. C. *Eur. Phys. J. B* **2010**, *78*, 411.

(24) Kurita, N.; Kimata, M.; Kodama, K.; Harada, A.; Tomita, M.; Suzuki, H. S.; Matsumoto, T.; Murata, K.; Uji, S.; Terashima, T. *Phys. Rev. B* **2011**, *83*, 214513.

(25) Mittal, R.; Mishra, S. K.; Chaplot, S. L.; Ovsyannikov, S. V.; Greenberg, E.; Trots, D. M.; Dubrovinsky, L.; Su, Y.; Brueckel, T.; Matsuishi, S.; Hosono, H.; Garbarino, G. *Phys. Rev. B* **2011**, *83*, 054503.

(26) Uhoya, W. O.; Montgomery, J. M.; Tsoi, G. M.; Vohra, Y. K.; McGuire, M. A.; Sefat, A. S.; Sales, B. C.; Weir, S. T. *J. Phys., Condens. Mater.* **2011**, *23*, 122201.

(27) Kawasaki, Y.; Mizuguchi, Y.; Deguchi, K.; Watanabe, T.; Ozaki, T.; Tsuda, S.; Yamaguchi, T.; Takeya, H.; Takano, Y. arXiv:1101.0896v1, 2011.

(28) Seyfarth, G.; Jaccard, D.; Pedrazzini, P.; Krzton-Maziopa, A.; Pomjakushina, E.; Conder, K.; Shermadini, Z. *Solid State Commun.* **2011**, *151*, 747.

(29) Subedi, A.; Zhang, L. J.; Singh, D. J.; Du, M. H. *Phys. Rev. B* **2008**, *78*, 134514.

(30) Ma, F. J.; Ji, W.; Hu, J. P.; Lu, Z. Y.; Xiang, T. *Phys. Rev. Lett.* **2009**, *102*, 177003.

(31) Kumar, A.; Kumar, P.; Waghmare, U. V.; Sood, A. K. *J. Phys., Condens. Mater.* **2010**, *22*, 385701.

(32) Singh, P. P. *J. Phys., Condens. Mater.* **2010**, *22*, 135501.

(33) Cao, C.; Dai, J. *Phys. Rev. B* **2011**, *83*, 193104.

(34) Shein, I. R.; Ivanovskii, A. L. arXiv:1102.3248v1, 2011.

(35) Yan, X.-W.; Gao, M.; LU, Z.-Y.; Xiang, T. arXiv:1102.2215v2, 2011.

(36) Hammersley, A. P. *ESRF Internal Report, ESRF97HA02T*; European Synchrotron Radiation Facility: Grenoble, France, 1997.

(37) Hammersley, A. P.; Svensson, S. O.; Hanfland, M.; Fitch, A. N.; Häusermann, D. *High Pressure Res.* **1996**, *14*, 235.

(38) Rodriguez-Carvajal, J. *IUCr Newsletter* **2001**, *26*, 12–19.

(39) Luo, X. G.; Wang, X. F.; Ying, J. J.; Yan, Y. J.; Li, Z. Y.; Zhang, M.; Wang, A. F.; Cheng, P.; Xiang, Z. J.; Ye, G. J.; Liu, R. H.; Chen, X. H. arXiv:1101.5670v1, 2011.

(40) Mizuguchi, Y.; Hara, Y.; Deguchi, K.; Tsuda, S.; Yamaguchi, T.; Takeda, K.; Kotegawa, H.; Tou, H.; Takano, Y. *Supercond. Sci. Technol.* **2010**, *23*, 054013.

(41) Paufler, P. *Acta Crystallogr.* **2007**, *A63*, 483.

(42) Kovalev, O. V. *Representations of the Crystallographic Space Groups: Irreducible Representations, Induced Representations and Corepresentations*, 2nd ed.; Gordon and Breach: New York, 1993.